

# Complex PQD Classification Using Time-Frequency Analysis and Multiscale Parallel Attention Residual Network

Jun Ma<sup>ID</sup>, *Student Member, IEEE*, Qiu Tang<sup>ID</sup>, Minjun He<sup>ID</sup>, Lorenzo Peretto<sup>ID</sup>, *Senior Member, IEEE*, and Zhaosheng Teng<sup>ID</sup>

**Abstract**—Accurate identification of complex power quality disturbances (PQDs) is highly important for the pollution control of modern power systems. However, the occurrence of nonlinear loads causes the grid signals distorted and unstable, resulting in the difficulty of efficient classification. This article aims to develop an effective detection method for complex PQD automatic classification. First, a modified Kaiser window-based S-Transform (MKS) is proposed for converting the PQD time-series signals to time-frequency feature matrix, where the time-frequency performance of MKS can be improved through setting different window control functions in low-frequency and high-frequency parts, respectively. Next, a multiscale parallel attention residual network (MPARN) is presented to extract and classify disturbance information based on the optimized residual structure. Integrating MKS and MPARN, an automatic classification framework is further proposed to identify various PQDs. Simulation and hardware platform experiments demonstrate that our classification strategy can obtain superior performance than several state-of-the-art methods for complex even nonlinear PQD identification under different noise levels.

**Index Terms**—Attention mechanism, convolutional neural network (CNN), power quality disturbances (PQD), residual networks (ResNets), time-frequency analysis.

Manuscript received 7 March 2023; revised 1 August 2023; accepted 5 October 2023. Date of publication 19 October 2023; date of current version 13 April 2024. This work was supported in part by the National Natural Science Foundation of China under Grant 52077067, in part by the Hunan Natural Science Foundation under Grant 2021JJ30124, in part by the Postgraduate Scientific Research Innovation Project of Hunan Province under Grant CX20220395, and in part by the China Scholarship Council under Grant 202206130054. (*Corresponding author: Zhaosheng Teng*.)

Jun Ma is with the College of Electrical and Information Engineering, Hunan University, Changsha 410082, China, and also with the Department of Electrical, Electronic and Information, University of Bologna, 40136 Bologna, Italy (e-mail: 19090277@hnu.edu.cn).

Qiu Tang and Zhaosheng Teng are with the College of Electrical and Information Engineering, Hunan University, Changsha 410082, China (e-mail: tangqiu@hnu.edu.cn; tengzs@hnu.edu.cn).

Minjun He is with the College of Electrical and Information Engineering, Hunan University, Changsha 410082, China, and also with the Department of Electrical, Electronic and Information, University of Bologna, 40136 Bologna, Italy (e-mail: mjun@hnu.edu.cn).

Lorenzo Peretto is with the Department of Electrical, Electronic and Information, University of Bologna, 40136 Bologna, Italy (e-mail: lorenzo.peretto@unibo.it).

Color versions of one or more figures in this article are available at <https://doi.org/10.1109/TIE.2023.3323692>.

Digital Object Identifier 10.1109/TIE.2023.3323692

## I. INTRODUCTION

IN RECENT years, power quality disturbance (PQD) events have occurred more and more frequently with the massive access to renewable energy [1], [2]. The power equipment and service are seriously disturbed by these distorted grid signals, thus, increasing the demand for a stable and clean grid environment [3]. Different from single disturbances, these PQD events often exist with multiple mixed disturbances in real-life power systems [4]. These mixed disturbances may be interrelated and cause failure features, which brings challenges for traditional PQD classification methods [5]. As the prerequisite of pollution control for the power grid, effective and reliable detection strategies for complex PQD identification need to be developed.

Nowadays, plenty of detection frameworks have been established for PQD identification. These frameworks generally consist of three parts: time-frequency analysis, feature extraction, and PQD classification [6]. The purpose of time-frequency analysis is to provide the joint distribution of both time domain and frequency domain for the PQD time-series signals. For instance, the short-time Fourier Transform (STFT) was deployed to provide the time-frequency information of transient disturbance in [7]. However, the time interval of STFT is fixed, resulting in the difficulty of distinguishing abrupt signals in complex PQDs. Other examples, including Hilbert–Huang Transform (HHT) [8], Wavelet Transform (WT) [9], and Stockwell Transform (ST) [10], are applied to improve the time-frequency resolution for PQD analysis. These time-frequency techniques have been widely used for PQD detection; however, some problems also need to be considered.

The WT provides variable time-frequency intervals compared with STFT; however, it lacks noise immunity, which limits its accuracy when detecting contaminated PQDs. The HHT can obtain higher time-frequency performance due to its outstanding antinoise ability, unfortunately, the calculation requirement is relatively high, especially for complex PQDs [11]. As the improved algorithm of STFT and WT, the ST provides more flexibility in time-frequency analysis [12]. However, insufficient energy concentration can easily cause disturbance information loss. To improve the energy concentration of ST, in the latest research, a Kaiser window-based S-Transform (KS) has been proposed in [13]. The KS can obtain more accurate time-frequency information by using a Kaiser window instead of a

traditional Gaussian window. However, the window parameters of KS are set empirically, which decreases its applicability for complex PQD signals.

Based on the time-frequency analysis result, the feature extraction and PQD classification can be further carried out [14]. Currently, the main ways for feature extraction include manual feature design-based and automatic feature extraction [15], [16]. For the former, some common manual features are extracted from the time-frequency information including the skewness, instantaneous harmonic distortion, and then, they are fed to the classifier [17]. For example, 12 types of disturbance features are selected manually to distinguish different PQDs by combining the extreme learning machine (ELM)-based classifier in [18]. In [19], only five types of disturbance features are considered and then fed to the support vector machine (SVM)-based classifier. Besides, over 20 types of disturbance features are conducted for the complex PQD detection in [20]. However, the classification pattern based on manual feature extraction often has some drawbacks. One is that the feature selection and feature number generally lack theoretical reference and may lead to information loss owing to human factors. The other is that the detection performance for complex PQDs will be limited if these manual features and classifiers do not match suitably [21]. Thus, more effective feature extraction and classification strategies need to be developed.

In recent years, with the development of convolutional neural network (CNN), PQD classification techniques based on automatic feature extraction are becoming increasingly popular [22]. For the automatic feature extraction, there is no need for the feature selection and all disturbance information is fed to the CNN-based classifier, which can effectively reduce information loss caused by the unsuitable feature design in the manual feature extraction process [23]. For instance, a multiple fusion CNN was proposed for automatic extraction and fusion of complex PQD features in [24]. In [21], a global depthwise shuffle CNN was conducted for PQD identification in some complicated phenomena. These automatic PQD detection strategies based on the CNN model contributed to the detection task of complex PQDs in modern power systems; however, the classification performance of CNN was directly affected by the feature validity. In [25], the attention mechanism was used for focusing the important feature information. Some related work was carried out to improve the classification performance of CNN by enhancing the feature significance based on attention mechanism [26], [27]. However, the application of attention-based CNN is limited to PQD classification. Besides, traditional network structure and feature extraction strategy based on a single convolutional kernel may result in information loss when handling complex PQD signals.

As a solution to the abovementioned problem, the main contributions of this article are listed as follows.

- 1) To improve the time-frequency resolution and adaptability for complex PQDs, a modified Kaiser window-based S-Transform (MKS) is presented to decompose PQD signals. In different frequency parts, the window parameters of MKS are variable and adjustable based on maximum energy concentration, which can provide

better time resolution at low frequencies while maintaining high-frequency resolution at high frequencies.

- 2) To further enhance the classification performance and reduce information loss, a multiscale parallel attention residual network (MPARN) is proposed to detect and identify complex PQDs. Based on the residual networks (ResNets) structure, two parallel convolutional layers are combined to extract and fuse multiscale feature information, and then, the attention mechanism is optimized to improve the representation power of disturbance features.
- 3) An automatic identification framework of complex PQDs is proposed based on MKS and MPARN. Instead of designing features manually, the identification process executes the disturbance feature extraction and classification automatically, which is proven to be a superior performance from the aspects of accuracy and robustness by extensive experiments.
- 4) The hardware platform for PQD detection is conducted to sample the experimental signal. Experimental results show that the time consumption of the MKS-MPARN is acceptable and can meet the real-time detection requirements of PQDs.

The rest of this article is organized as follows. Section II first proposes the PQD detection framework MKS-MPARN. The principle of the MKS is introduced in Section III. In Section IV, the detail of the MPARN is described. Then, experiments are conducted in Section V. Finally, Section VI concludes this article.

## II. WORKFLOW FOR COMPLEX PQD CLASSIFICATION

To achieve effective and reliable detection for complex PQDs, this research proposes a novel classification framework by combining the MKS technique and the MPARN model. The MKS is deployed for disturbance time-frequency analysis, which aims to extract more accurate time-frequency information. Then, the MPARN is used as a classifier to identify different disturbance features automatically. The parameters of MPARN are optimized by using the grid search. The workflow of MKS-MPARN is shown in Fig. 1. The corresponding introduction is listed as follows.

- 1) *Signal Time-Frequency Analysis:* The time-series PQD signals with different noises are transformed into time-frequency-amplitude matrix  $\text{MKS}_A(m, n)$ . A double-resolution strategy is considered to analyze different types of disturbances pertinently. Besides, the window parameters in the MKS can be optimized adaptively to obtain the optimal energy concentration.
- 2) *Complex PQD Classification:* The matrix  $\text{MKS}_A(m, n)$  is fed into MPARN to achieve the feature extraction and identification of PQDs. In the weight layer 1, the multiscale parallel convolution is deployed to enrich the extracted feature information. Then, the attention module is carried out in the weight layer 2 to improve the representation power of the PQD feature. The convolution with size  $1 \times 1$  is used in the skip connection to fit the feature dimension. The kernel size of all pooling

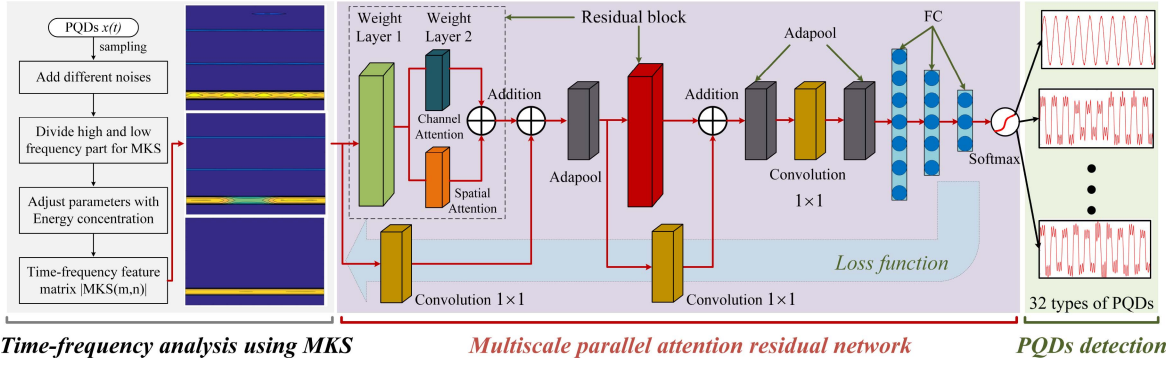


Fig. 1. Workflow of the MKS-MPARN for complex PQD classification.

layers is  $2 \times 2$  in this research, which is used for the feature downsampling. All activation functions, including convolution layers and three fully connected (FC) layers, are set to the parametric rectified linear unit (PReLU) [28]. The whole classification process is automatic without empirical feature design.

Thereby, the specific descriptions for the proposed MKS and MPARN are presented in the next sections.

### III. MODIFIED KS

#### A. Motivation

The feature information of disturbance is significant for the accurate detection of complex PQDs. Thus, the time–frequency analysis should provide a high time and frequency resolution as soon as possible. However, the traditional S-Transform based on the Gaussian window is hard to meet this requirement due to its low-energy concentration. In the latest research, a KS [13] was proposed to overcome this limitation of ST, which can be defined as

$$\text{KS}(\tau, f) = \int_{-\infty}^{+\infty} x(t)w(\tau - t, f)e^{-i2\pi ft}dt \quad (1)$$

where  $x(t)$  is the PQD signal with the fundamental frequency  $f_0$ ,  $\tau$  denotes time shift factor,  $f$  is signal frequency, and  $w(t, f)$  is Kaiser window function, which can be defined as

$$w(t, f) = \frac{I_0[\beta(f)\sqrt{1 - (t/T)^2}]}{I_0[\beta(f)]}, |t| \leq T \quad (2)$$

where  $\beta(f)$  denotes the control function of Kaiser window,  $T$  is signal period,  $I_0(\cdot)$  represents the first kind of zeroth-order Bessel function, and its series expression is

$$I_0(\cdot) = 1 + \sum_{p=1}^{\infty} \left[ \frac{(\cdot/2)^p}{p!} \right]. \quad (3)$$

The KS works perfectly for most PQD signals due to its satisfactory energy concentration. However, the single control function makes it difficult to obtain excellent time resolution and frequency resolution simultaneously. Besides, the fixed window parameters limit its adaptability for complex and changeable

PQDs. To address this, the MKS is proposed to further optimize the adaptation and improve the time–frequency resolution of KS.

#### B. Proposed MKS

To balance the time and frequency resolution of KS, motivated by Li et al. [6], the MKS is first to divide the time–frequency spectrum of PQDs into two parts, namely low-frequency part and high-frequency part. In the low-frequency part,  $f \leq 1.5f_0$ , the disturbances mainly include Swell, Sag, Flicker, and so on, which require an accurate time resolution and the high-frequency part,  $f > 1.5f_0$ , mainly contains Harmonics and Transient, which needs a high-frequency resolution.

Then, we can improve both the time resolution and frequency resolution in different frequency parts by using different control functions. Instead of the single  $\beta(f)$ , the control function in this article is replaced by  $\gamma(f)$ , which can be described as

$$\gamma(f) = \begin{cases} \frac{\xi_1}{f + \xi_2} & \text{if } f \leq 1.5f_0 \\ \frac{\xi_3}{f + \xi_4} & \text{if } f > 1.5f_0 \end{cases} \quad (4)$$

where  $\xi$  is the control factor, a higher  $\xi_1$  can obtain better time resolution in the low-frequency part while a lower  $\xi_3$  can provide more accurate frequency resolution in the high-frequency part, and  $\xi_2$  and  $\xi_4$  can more easily smooth the change rate of window shape.

Based on the new control function  $\gamma(f)$ , the MKS can be further expressed as

$$\text{MKS}(\tau, f)$$

$$= \int_{-\infty}^{\infty} x(t) \frac{I_0[\gamma(f)\sqrt{1 - ((t - \tau)/T)^2}]}{I_0[\gamma(f)]} e^{-i2\pi ft} dt. \quad (5)$$

The sampling rate of PQD signals is set to  $f_s$ , and the sampling point is set to  $N$ . We set  $\tau = mT_s$ ,  $f = nf_s/N$ , when  $n > 0$ , the discrete MKS of  $x(n)$  can be expressed as

$$\text{MKS}(m, n) = \sum_{k=0}^{N-1} X(n+k)W(n)e^{j\frac{2\pi mk}{N}} \quad (6)$$

where  $X(n+k)$  is the discrete Fourier transform of  $x(n)$  and  $W(n)$  denotes the Fourier spectrum of Kaiser window  $w'(f)$ . Considering the diversity and complexity of the PQDs, an adaptive adjustment strategy for the control factors is necessary. Motivated by the authors in [12] and [29], the measurement of energy concentration for the discrete MKS can be expressed by

$$E(\xi_1, \xi_2, \xi_3, \xi_4) = \frac{1}{\sum_{m=1}^M \sum_{n=1}^N \left| \frac{\text{MKS}(m,n)}{\sqrt{\sum \sum |\text{MKS}(m,n)|^2}} \right|} \quad (7)$$

where the matrix  $\text{MKS}(m, n)$  is of size  $M \times N$ .

We set the  $E_{\text{MKS}}$  as the reciprocal of energy concentration value. The goal of MKS is to provide better time and frequency resolution with high energy concentration. Therefore, the optimization goal is to minimize the  $E_{\text{MKS}}$  and the optimization problem for the parameters adjustment of MKS can be defined as

$$\begin{aligned} & \arg \min_{\xi_1, \xi_2, \xi_3, \xi_4} \{E_{\text{MKS}}(\xi_1, \xi_2, \xi_3, \xi_4)\} \\ & \text{s.t. } \xi_1 > \xi_3 > 0 \\ & \quad \xi_4 > \xi_2 \geq 0. \end{aligned} \quad (8)$$

Then, (8) is selected as the fitness function, and we can solve this nonlinear optimization problem by referring to [30]. In this work, the fundamental wave frequency  $f_0$ , the sampling frequency  $f_s$ , and the sampling time are 50 Hz, 6400 Hz, and 0.2 s, respectively. It means that the PQD signals are sampled for ten periods.

In fact, MKS is a complex-valued matrix, which can be described as

$$\text{MKS}(m, n) = |\text{MKS}(m, n)| e^{j\phi(m, n)} \quad (9)$$

where  $|\text{MKS}(m, n)|$  and  $\phi(m, n)$  are the amplitude and phase angle of  $\text{MKS}(m, n)$ , respectively. For simplicity, the  $\text{MKS}_A(m, n) = |\text{MKS}(m, n)|$  represents the amplitude matrix of MKS in time–frequency analysis.

### C. Signal Analysis Using MKS

To prove that the proposed MKS can provide better time resolution at low frequencies while maintaining high-frequency resolution at high frequencies, two types of complex PQDs are conducted as the case study. One is the Sag + Spike + Harmonics, which aims to validate the time resolution at low frequencies. The other is Flicker + Harmonics + Transient, which aims to verify the frequency resolution at high frequencies. The PQD signals and corresponding time–frequency results based on the MKS are shown in Fig. 2.

To decrease the time consumption of the MKS, referring to [6], just some important frequency points including fundamental frequency, harmonic frequencies, and their nearby two points are calculated. From Fig. 2(b), the proposed MKS has a better time resolution at low frequencies, which can effectively detect the start and ending time of the Sag and Spike while superimposing the Harmonics. From Fig. 2(d), the MKS also maintains a high-frequency resolution at high frequencies, which can identify the Harmonics and Transient with different

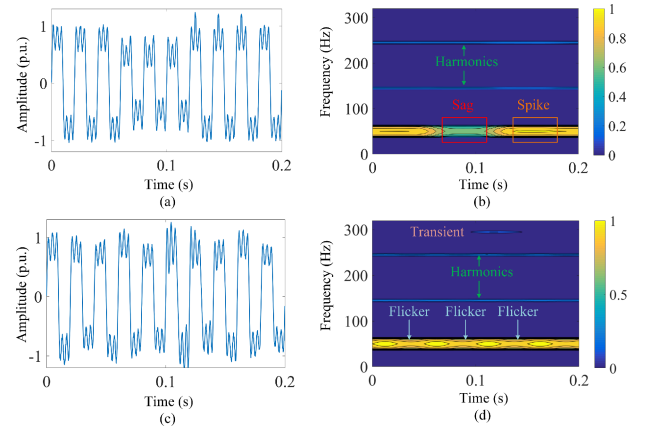


**Fig. 2.** Time–frequency analysis result of MKS on complex PQDs. (a) Disturbance signal: Sag + Spike + Harmonics. (b) MKS of (a). (c) Disturbance signal: Flicker + Transient + Harmonics. (d) MKS of (c).

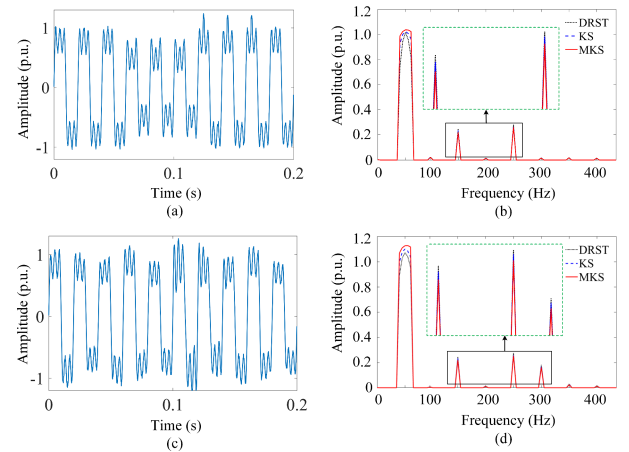


**Fig. 3.** Comparison results on frequency–amplitude performance and energy concentration. (a) Disturbance signal: Sag + Spike + Harmonics. (b) Frequency–amplitude curves of (a),  $E_{\text{MKS}} = 89.90$ ,  $E_{\text{KS}} = 90.67$ , and  $E_{\text{DRST}} = 91.65$ . (c) Disturbance signal: Flicker + Transient + Harmonics. (d) Frequency–amplitude curves of (c),  $E_{\text{MKS}} = 90.31$ ,  $E_{\text{KS}} = 91.16$ , and  $E_{\text{DRST}} = 92.04$ .

frequencies while superimposing the Flicker. The disturbance information becomes more clear and prominent after the time–frequency analysis provided by MKS, which can contribute to the automatic classification of PQDs.

Specially, to validate the time–frequency performance of the MKS, the DRST [6] and KS [13] are selected as a comparison. The frequency–amplitude curves of these three time–frequency algorithms for PQDs are shown in Fig. 3. From Fig. 3, the energy intensity of the MKS in the fundamental frequency is higher than those of the DRST and KS, indicating a higher time–frequency energy concentration. Besides, the  $E_{\text{MKS}}$  of MKS in Fig. 3(b) and (d) are 89.90 and 90.31, respectively, while those of KS and DRST are 90.67 and 91.16, and 91.65 and 92.04, respectively. It quantitatively reflects that the energy concentration of KS and MKS is higher than that of DRST, demonstrating Kaiser window can provide an optimal time–frequency performance than that of the Gaussian window. The MKS outperforms the

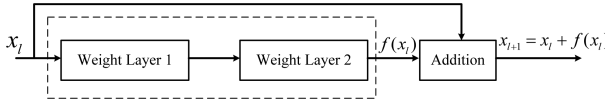


Fig. 4. Primary structure of identity mapping in ResNets.

KS, proving that the proposed control function  $\gamma(f)$  is more adaptive for complex PQD analysis than the original  $\beta(f)$ .

After obtaining the time–frequency information of PQDs, an effective classifier is needed to automatically classify complex disturbance signals. Next, an MPARN will be described as a classifier for the automatic identification of complex PQDs.

#### IV. MULTISCALE PARALLEL ATTENTION RESNET

Considering the excellent feature grabbing and classification ability of CNN, after the time–frequency analysis, the CNN-based model is developed for the automatic detection and identification of complex PQDs.

##### A. ResNet Structure

The ResNets, as an improvement structure of CNN, have been proven that it has satisfactory optimization and feature expression ability for PQD analysis [31]. The principle of ResNets [32] is to propagate information combined with skip connections, which can effectively avoid gradient vanishing and improve accuracy. The primary structure of identity mapping in ResNets is shown in Fig. 4.

From Fig. 4, the primary identity mapping is defined as

$$x_{l+1} = x_l + f(x_l) \quad (10)$$

where  $x_l$  and  $x_{l+1}$  represent the input and output features of residual unit, respectively, and  $f(x_l)$  represents the output feature after feature extraction by two weight layers.

Based on (10), the backpropagation form in residual unit can be expressed as

$$\frac{\partial \ell}{\partial x_l} = \frac{\partial \ell}{\partial x_{l+1}} \frac{\partial x_{l+1}}{\partial x_l} = \frac{\partial \ell}{\partial x_{l+1}} \left( 1 + \frac{\partial f(x_l)}{\partial x_l} \right) \quad (11)$$

where the  $\ell$  is the loss function. It shows that the gradient of the residual unit will not vanish, even  $\frac{\partial f(x_l)}{\partial x_l}$  is close to 0.

Generally, the weight layer in Fig. 4 is a single convolutional layer, namely, the feature extraction is achieved by two sequential convolutional operations. It is effective when the ResNets structure is enough deep. However, considering the real-time requirement for PQD classification, we should make the network structure shallow as much as possible. It means that the effect of ResNets will not be significant if we still use the single convolutional layer as a weight layer for feature extraction. To address this, an MPARN is proposed to improve the performance of ResNets in shallow structures.

##### B. Structure of Proposed MPARN

Considering the importance of the weight layer, based on [33], the first improvement of MPARN is using two parallel convolutional layers with different sizes to extract and fuse the

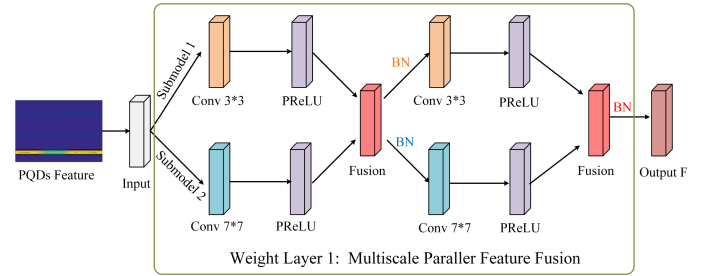


Fig. 5. Multiscale feature fusion structure in weight layer 1.

high-dimensional and low-dimensional features simultaneously from two submodels in weight layer 1. The structure of weight layer 1 is shown in Fig. 5.

In Fig. 5, it can be seen that the PQD feature is extracted from two submodels. The submodel 1 with the convolutional kernel size  $3 \times 3$  is used to extract the low-dimensional feature information and the submodel 2 is used to obtain high-dimensional feature information. The output of the convolutional layer is described as

$$Z_c = f(W^r * X_m + b^r) \quad (12)$$

where  $W^r = \{W_l^r, W_h^r\}$  represents the weight of convolutional kernel for submodel 1 and submodel 2 in the  $r$ th, respectively,  $b^r = \{b_l^r, b_h^r\}$  denotes the bias term, and  $*$  represents the convolutional operator. To improve the adaptation of the rectifiers and enhance accuracy at negligible extra time consumption, referring to [28], the PReLU is used to replace the ReLU as activate function  $f$ , defined as

$$\text{PReLU}(x_i) = \begin{cases} x_i, & \text{if } x_i > 0 \\ \alpha_i x_i, & \text{if } x_i \leq 0 \end{cases} \quad (13)$$

where  $\alpha_i$  controls the slope of the negative part in the  $i$ th channel. Besides,  $\alpha_i$  is a learnable parameter, which can be updated simultaneously with other layers by using backpropagation.

To enrich PQD feature information, we then fuse these features from two submodels. This process is called the fusion layer in this article. It is worth mentioning that features from two submodels should have equal dimensions before fusion. This can be achieved through the padding operation. Suppose the features in the  $r$ th fusion layer is  $C^r$ , it can be defined as

$$\begin{aligned} C^r &= f(W_l^r * X_m + b_l^r) + f(W_h^r * X_m + b_h^r) \\ &= Z_c^l + Z_c^h. \end{aligned} \quad (14)$$

From (14), it shows that the fusion layer conducts a stronger disturbance feature than each submodel. Compared with a single submodel, these two different scale features complement each other, which is highly useful to provide more complete disturbance information even if one of them is weak.

To accelerate the computational time and reduce overfitting, batch normalization (BN) is introduced to adjust the output of the fusion layer as a new Gaussian distribution [34]. After two fusion operations in weight layer 1, the PQD feature is fully

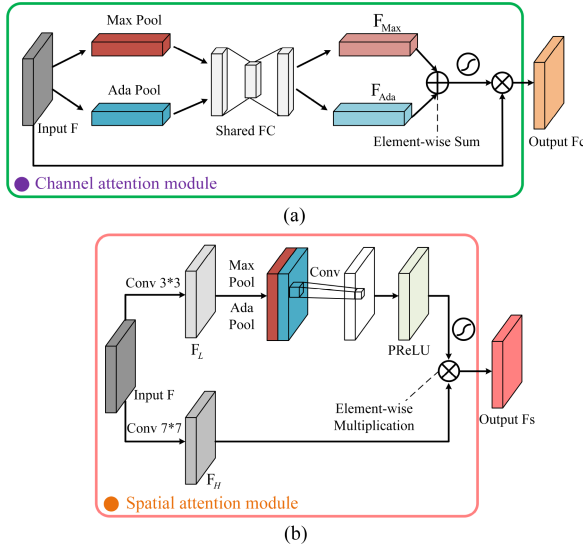


Fig. 6. Design of attention block in weight layer 2. (a) Channel attention module. (b) Spatial attention module.

extracted and then can be set as the input of the weight layer 2 for disturbance identification.

Different from the traditional residual unit, the main goal of weight layer 2 in MPARN is to significantly increase the representation power of the disturbance feature provided by weight layer 1. Motivated by Woo et al. [26], the attention modules are placed following BN layers as the weight layer 2, which is lightweight and has a low time consumption. Particularly, instead of the average-pooling to aggregate spatial information in [26], the AdaPool [35] is introduced to combine with max-pooling for conducting attention block. Compared with average-pooling, the AdaPool can improve the preservation of detail and reduce information loss. The design of the attention layer in MPARN is shown in Fig. 6.

From Fig. 6, the attention layer contains parallel channel attention and spatial attention modules, which are shown in Fig. 6(a) and (b), respectively. It is worth mentioning that the sequential manner for these two attention modules is also feasible, the specific selection is based on the actual case study. In this research, the parallel manner has a higher accuracy than the sequential manner, which is the reason for determining the parallel manner in the weight layer 2. The channel attention is developed to reveal the interchannel relationship of disturbance features. The spatial information of input feature map  $F \in \mathbb{R}^{C \times H \times W}$  provided by weight layer 1 is extracted by Adapool and max-pooling to denote the comprehensive and distinctive feature information, respectively, and as the input of a shared FC layer. Then, two attention maps  $F_{\text{Ada}}$  and  $F_{\text{Max}}$  are obtained and merged to produce the channel attention  $A_c \in \mathbb{R}^{C \times 1 \times 1}$ . Finally, the elementwise multiplication is carried out on the channel attention and input feature map to achieve the final channel attention map,  $F_c \in \mathbb{R}^{C \times H \times W}$ . The whole process can be described as

$$\begin{cases} A_c = \sigma(\text{FC}(\text{Ada}(F)) + \text{FC}(\text{Max}(F))) \\ F_c = A_c \otimes F \end{cases} \quad (15)$$

where  $\sigma$  is Sigmoid function, FC denotes the shared FC layer, and Ada and Max represent Adapool and max-pooling operation, respectively.

In the spatial attention module, specially, we design two different size convolutional layers to extract the disturbance information, where the conv  $3 \times 3$  and the conv  $7 \times 7$  are used to extract the low-level feature  $F_L$  and high-level feature  $F_H$ , respectively. The conv  $7 \times 7$  has a higher receptive field and aims to focus on the global feature information. In comparison, the conv  $3 \times 3$  can obtain more detailed information and is used to extract local features. Based on the characteristics of the conv  $3 \times 3$  and the conv  $7 \times 7$ , the spatial attention is added into conv  $3 \times 3$  to emphasize important detailed information. Then, the Adapool and max-pooling are applied to  $F_L$  to generate 2-D maps:  $F_L^{\text{Ada}} \in \mathbb{R}^{1 \times H \times W}$  and  $F_L^{\text{Max}} \in \mathbb{R}^{1 \times H \times W}$ , which can denote different pooling features across the channel and enhance the network representation power. Those are concatenated and fed into a convolutional layer to produce spatial attention,  $A_s \in \mathbb{R}^{1 \times H \times W}$ . Finally, the elementwise multiplication is performed on the high-level feature  $F_H$  and the spatial attention to create the effective spatial attention map,  $F_s \in \mathbb{R}^{C \times H \times W}$ . Through this way, the low-level feature  $F_L$  can help the MPARN focus on appropriate high-level feature  $F_H$  and improve the performance of PQD detection. This process can be expressed as

$$\begin{cases} A_s = \sigma[\text{Conv}_{3 \times 3}\{\text{Concat}(\text{Ada}(F_L), \text{Max}(F_L))\}] \\ F_s = A_s \otimes F_H \end{cases} \quad (16)$$

where Conv<sub>3×3</sub> denotes a convolution operation with size of  $3 \times 3$  and Concat is the concatenation operation.

According to above introduction, it can be known that the weight layer 1 is deployed to enrich the PQD feature information using multiscale feature fusion, and the weight layer 2 is developed to emphasize the significant feature information based on the optimization of channel attention module and spatial attention module. Then, the residual unit of MPARN can be conducted based on the combination of weight layer 1 and weight layer 2, which can highly improve the classification performance of MPARN.

## V. EXPERIMENTS AND EVALUATIONS

To validate the PQD detection performance of the proposed MKS-MPARN framework, multiple comprehensive experiments, including simulation and hardware platform experiments, are carried out in this part. The verification aspects contain the classification accuracy, robustness, and real-time performance for different disturbance signals.

### A. PQDs Data

To make the classification result more convincing, 32 types of PQDs are generated, including nine single PQDs and 21 complex PQDs based on IEEE-1159 standards [36] and reference [37]. Considering the complexity of nonlinear loads in real-power systems, referring to [21], two types of nonlinear PQDs are also tested for robustness verification. Differing from traditional disturbances, nonlinear PQDs are constructed by multiplying

**TABLE I**  
32 TYPES OF PQDs

Class	PQ Disturbance	Class	PQ Disturbance
C1	Normal	C17	Swell + Transient
C2	Sag	C18	Spike + Transient
C3	Swell	C19	Notch + Transient
C4	Interrupt	C20	Flicker + Sag
C5	Harmonics	C21	Transient + Harmonics + Sag
C6	Transient	C22	Transient + Harmonics + Swell
C7	Flicker	C23	Transient + Harmonics + Interrupt
C8	Notch	C24	Transient + Harmonics + Flicker
C9	Spike	C25	Flicker + Harmonics + Interrupt
C10	Spike + Harmonics	C26	Flicker + Harmonics + Sag
C11	Sag + Harmonics	C27	Flicker + Harmonics + Swell
C12	Swell + Harmonics	C28	Spike + Harmonics + Sag
C13	Interrupt + Harmonics	C29	Spike + Harmonics + Interrupt
C14	Transient + Harmonics	C30	Spike + Harmonics + Swell
C15	Flicker + Harmonics	C31	<b>Transient with Swell</b>
C16	Sag + Transient	C32	Flicker with Transient

**TABLE II**  
ACCURACY COMPARISON UNDER DIFFERENT NOISE LEVELS

Method	Classifier	Accuracy (%)			
		Clean	10 dB	20 dB	40 dB
DRST	MPARN	99.13	87.58	98.03	98.96
OST	MPARN	99.20	88.01	98.87	99.17
KS	MPARN	99.55	89.43	99.16	99.31
MKS	WRN	99.27	88.03	98.65	99.12
MKS	MPRN	99.48	89.11	99.04	99.19
MKS	<b>MPARN</b>	<b>99.76</b>	<b>91.07</b>	<b>99.42</b>	<b>99.70</b>

The bold entities emphasize the proposed method.

different disturbance components. All these 32 kinds of composite PQDs are listed in Table I.

The fundamental frequency of disturbance is 50 Hz. The sampling rate and sampling time are 6400 Hz and 0.2 s, respectively. In total, 3000 samples per disturbance are generated in MATLAB, where the training set, verification set, and test set account for 60%, 20%, and 20%, respectively. The implementation of the training process for MPARN is on the Pytorch framework. The graphics processing unit (GPU) hardware platform is GTX 1650.

### B. Performance Verification Under Different Noise Levels

The proposed classification framework consists of the MKS and MPARN, where the MKS is used for time–frequency analysis and the MPARN for PQD classification. To verify the performance of the proposed MKS and MPARN, respectively, different comparison experiments are carried out. For the MKS, some representative methods, including DRST [6], optimized S-transform (OST) [17], and KS [13], are picked as the comparison. To show the improvement in the accuracy of MKS, these examined time–frequency methods are also combined with the proposed MPARN, namely MKS-MPARN, DRST-MPARN, and so on. For the MPARN, a weighted residual network (WRN) [31] is selected as a comparison. Besides, the MPRN is conducted to validate the attention module in MPARN. These examined ResNets are combined with the proposed MKS for a fair comparison. The comparison result under different noise levels is given in Table II.

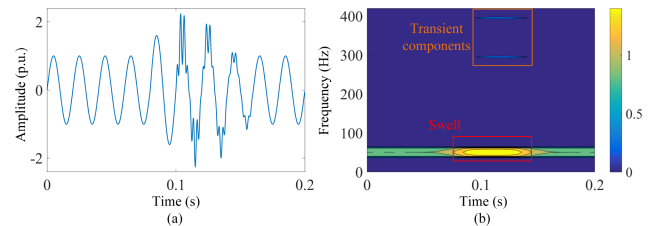


**Fig. 7.** Time–frequency analysis for the nonlinear disturbance of Transient with Swell.

**TABLE III**  
ACCURACY FOR NONLINEARLY MIXED PQDS

Nonlinearly mixed PQDs	Accuracy (%)		
	Clean	20 dB	40 dB
Transient with swell	99.5	98.83	99.17
Flicker with transient	99.67	99.0	99.5

Note that the classification result represents the classification average accuracy for 32 types of PQDs. It can be seen from Table II that the accuracy of these examined frameworks increases with the increase of the noise level, indicating the noise level directly affects the classification result. Besides, the accuracy of KS and MKS is higher than the DRST and OST, indicating the Kaiser window could provide a higher time–frequency performance. The MKS outperforms the KS, proving that the dynamic parameter adjustment in different frequency parts can enhance the adaptation of MKS for complex PQDs. In addition, for these examined classifiers, the MPRN has higher accuracy than the WRN, which demonstrates the parallel convolutional layers in the weight layer 1 can obtain more comprehensive feature information. The proposed MPARN outperforms the MPRN, indicating that the attention structure in the weight layer 2 can further improve the feature representation power of MPRN. Even under the 10 dB noise level, the proposed MKS-MPARN can obtain 91.07% accuracy, which shows a satisfactory antinoise performance and excellent classification accuracy.

Specially, we list the classification accuracy of MKS-MPARN for two types of nonlinear disturbances. Take the class of C31 Transient with Swell as the display, the time–frequency analysis result by the MKS is shown in Fig. 7. From Fig. 7, it can be seen that the transient components can be effectively detected. Besides, the Swell in the fundamental frequency is obvious. The time–frequency analysis result demonstrates that the MKS is also suitable for detecting nonlinear disturbances. The classification result of the MKS-MPARN for these nonlinear disturbances is given in Table III. From Table III, it can be observed that the accuracy of MKS-MPARN is higher than 99% when noise level is 40 dB. It can still obtain 98.83% accuracy under the 20 dB noise level, which proves that the MKS-MPARN framework has an outstanding robustness to identify some more complex nonlinear PQDs.

**TABLE IV**  
PERFORMANCE COMPARISON WITH OTHER TECHNIQUES

Framework	Types of PQDs	Feature Extraction	SNR (dB)	Accuracy (%)
TQWT + MSVM [19]	14	Manual	20	96.42
ST + NSGA-II [20]	15	Manual	20	96.43
HT + slip-SVDNSA [38]	11	Manual	20	98.45
DRST + DAG-SVM [6]	9	Manual	30	97.77
HHT + WBELM [18]	16	Manual	20	99.00
VMD + DT [15]	14	Manual	30	96.73
DWT + RF [14]	21	Manual	clear	96.21
ACMP + GOA-SVM [39]	16	Manual	20	97.13
OST + KSVM [17]	24	Automatic	20	98.82
EITD + GSCNN [21]	27	Automatic	20	98.56
MFCNN [24]	24	Automatic	20	99.26
<b>MKS-MPARN</b>	<b>32</b>	<b>Automatic</b>	<b>20</b>	<b>99.42</b>

The bold entities emphasize the proposed method.

### C. Classification Performance Comparison

To validate the classification performance of our MKS-MPARN, MKS-MPARN is compared with some recently proposed classification frameworks, as listed in Table IV. It is worth mentioning that the “Manual” represents disturbance features that need to be designed according to experience. The “Automatic” indicates that the classification framework automatically achieves the PQD identification without feature selection.

From Table IV, it can be given that the PQD classification framework based on the “Automatic” model can obtain higher average accuracy than that of “Manual” model. For example, the accuracy of these “Automatic” models is higher than 98% while most of the “Manual” models are lower than 98%, indicating that automatic feature extraction helps reduce information loss and is more suitable for PQD classification. Also, it can be noticed that HHT-WBELM [18] can reach 99.0%; however, it only considers 16 types of disturbances, which may not be enough to reflect its generalization performance. By improving the time–frequency performance and network feature extraction power, the proposed MKS-MPARN can obtain 99.42% accuracy under 20 dB noise. More importantly, it has an excellent robustness performance for identifying nonlinear disturbances.

### D. Experimental Verification Analysis

The practicability of the MKS-MPARN is highly important for the actual PQD detection. To further verify the classification performance of the proposed MKS-MPARN under experimental signals, referring to some related works [2], [5], a hardware platform with signal real-time acquisition card is designed for PQD sampling. The hardware platform is shown in Fig 8. As shown in Fig. 8, the hardware platform consists of three parts: disturbance signal source Fluke 6105 A, signal acquisition card NI 9222, and PC.

Limited by the function output of Fluke 6105 A, the experimental PQD signals contain six types of single PQDs, namely, C1, C2, C3, C4, C5, and C7. Based on these single PQDs, the corresponding six types of complex PQDs are further conducted, including C11, C12, C15, C25, C26, and C27. After being preheated for some time, the Fluke 6105 A randomly generates different PQDs. Then, PQD signals are sampled and transmitted to the computer in real time through the acquisition card NI

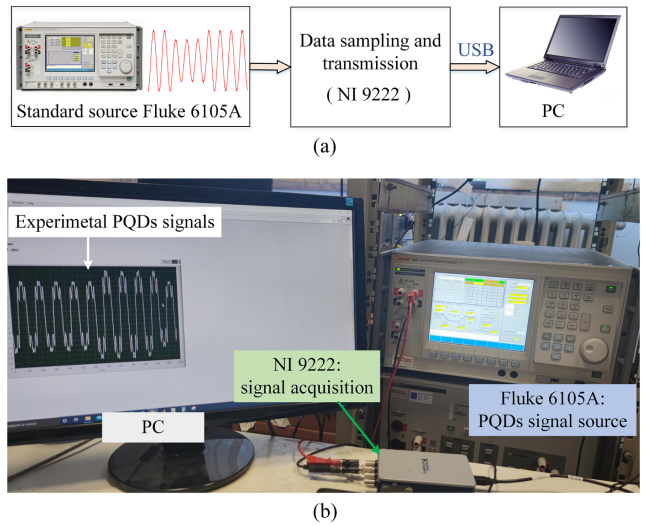


**Fig. 8.** PQD sampling hardware platform. (a) Signal acquisition process, (b) Hardware platform.

**TABLE V**  
ACCURACY UNDER THE EXPERIMENTAL SIGNALS

Class	Accuracy (%)	Average accuracy (%)	Test time per sample (ms)
C1	100		
C2	97.50		
C3	98.75		
C4	98.75		
C5	97.50		
C7	97.50		
C11	96.25	97.40	140
C12	97.50		
C15	96.25		
C25	97.50		
C26	95.00		
C27	96.25		

9222. The sampling frequency is set to 6400 Hz. The number of sampling points is 1280 per PQD, namely ten periods. The sampling time is 200 ms.

For each type of PQD, 80 samples are tested, and the results are given in Table V. As can be seen from Table V, the accuracy for complex PQDs is a bit lower than that of single PQDs, which demonstrates that the disturbance mixture increases the detection difficulty. The average accuracy of MKS-MPARN for experimental PQDs can still reach 97.40%, proving an excellent classification accuracy. In addition, the test time per sample is 140 ms, which is lower than 200 ms, indicating the time consumption of the MKS-MPARN is acceptable and it can meet the real-time requirements for PQD detection. Therefore, the proposed MKS-MPARN can provide a satisfactory classification performance under experimental PQD signals.

Besides, to validate the superiority of our MKS-MPARN, some other classification methods in the simulation experiments are selected for further comparison. The comparison result is listed in Table VI. From Table VI, the classification result for the experimental signals shows that the automatic feature extraction-based framework can obtain a higher accuracy. For

**TABLE VI**  
ACCURACY COMPARISON UNDER THE EXPERIMENTAL PQD SIGNALS

Framework	Feature extraction	Average accuracy (%)
ACMP+GOA-SVM [39]	Manual	95.73
HHT + WBELM [18]	Manual	96.46
OST + KSVM [17]	Automatic	96.67
MFCNN [24]	Automatic	96.98
MKS-MPARN	Automatic	97.40

example, the MFCNN can reach 96.98% accuracy while those of GOA-SVM and WBELM are 95.73% and 96.46%, respectively. The proposed MKS-MPARN has the highest classification accuracy 97.40%, proving its superiority for complex PQD identification.

## VI. CONCLUSION

In this article, a MKS and MPARN were proposed for the real-time classification of single and complex PQDs. The proposed MKS improved KS by using different window control functions in high-frequency and low-frequency parts. Besides, the parameters could be optimized by maximizing the energy concentration of MKS. The experimental results showed that the MKS performs better than some popular time–frequency methods and could provide more accurate time–frequency information for disturbance detection. Then, an MPARN was proposed to learn and extract this disturbance information automatically. The feature representation power of PQDs could be significantly improved through the combination of parallel convolution fusion and attention layer in residual structure. Different experiments were conducted and the result demonstrated that the MKS-MPARN had higher accuracy and antinoise performance than some recently proposed detection techniques. Moreover, it was robust for nonlinear PQDs. Finally, experiments on the PQD hardware platform proved that MKS-MPARN had a satisfactory accuracy and real-time performance.

Besides, the PQD signals could be also transformed separately for low and high frequencies to produce two MKSs in the time–frequency analysis stage. However, this way had a high time consumption and could not meet the real-time detection requirement in our framework. In our future work, we will explore the improvement method for time–frequency optimization and network structure simplification. Then, maybe it is possible to produce two MKSs for a more effective PQD identification.

## REFERENCES

- Cui, Y., Duan, H., Hu, L., Wang, and Q. Liu, "Detection and classification of multiple power quality disturbances using stockwell transform and deep learning," *IEEE Trans. Instrum. Meas.*, vol. 71, 2022, Art. no. 2519912.
- Iturriño-García et al., "An innovative single shot power quality disturbance detector algorithm," *IEEE Trans. Instrum. Meas.*, vol. 71, 2022, Art. no. 2517210.
- Liu, T., Jin, M. A., Mohamed, and Q. Wang, "A novel three-step classification approach based on time-dependent spectral features for complex power quality disturbances," *IEEE Trans. Instrum. Meas.*, vol. 70, 2021, Art. no. 3000814.
- Z. Liu, Y. Cui, and W. Li, "A classification method for complex power quality disturbances using EEMD and rank wavelet SVM," *IEEE Trans. Smart Grid*, vol. 6, no. 4, pp. 1678–1685, Jul. 2015.
- D. Gu, Y. Gao, Y. Li, Y. Zhu, and C. Wu, "A novel label-guided attention method for multilabel classification of multiple power quality disturbances," *IEEE Trans. Ind. Informat.*, vol. 18, no. 7, pp. 4698–4706, Jul. 2022.
- J. Li, Z. Teng, Q. Tang, and J. Song, "Detection and classification of power quality disturbances using double resolution S-transform and DAG-SVMs," *IEEE Trans. Instrum. Meas.*, vol. 65, no. 10, pp. 2302–2312, Oct. 2016.
- K. Satpathi, Y. M. Yeap, A. Ukil, and N. Geddada, "Short-time fourier transform based transient analysis of VSC interfaced point-to-point DC system," *IEEE Trans. Ind. Electron.*, vol. 65, no. 5, pp. 4080–4091, May 2018.
- J. Zheng et al., "Time-frequency analysis of scalp EEG with Hilbert-Huang transform and deep learning," *IEEE J. Biomed. Health Informat.*, vol. 26, no. 4, pp. 1549–1559, Apr. 2022.
- M. D. Borr, J. C. Bravo, and J. C. Montao, "Disturbance ratio for optimal multi-event classification in power distribution networks," *IEEE Trans. Ind. Electron.*, vol. 63, no. 5, pp. 3117–3124, May 2016.
- L. Pan, Z. Han, X. Wenxu, and J. Qingquan, "A fast adaptive S-transform for complex quality disturbance feature extraction," *IEEE Trans. Ind. Electron.*, vol. 70, no. 5, pp. 5266–5276, May 2023.
- W. Qiu, Q. Tang, J. Liu, Z. Teng, and W. Yao, "Power quality disturbances recognition using modified S transform and parallel stack sparse auto-encoder," *Electric Power Syst. Res.*, vol. 174, 2019, Art. no. 105876.
- M. V. Reddy and R. Sodhi, "A modified S-transform and random forests-based power quality assessment framework," *IEEE Trans. Instrum. Meas.*, vol. 67, no. 1, pp. 78–89, Jan. 2018.
- C. Liang et al., "A Kaiser window-based S-transform for time-frequency analysis of power quality signals," *IEEE Trans. Ind. Informat.*, vol. 18, no. 2, pp. 965–975, Feb. 2022.
- M. Markovska, D. Taskovski, Z. Kokolanski, V. Dimchev, and B. Velkovski, "Real-time implementation of optimized power quality events classifier," *IEEE Trans. Ind. Appl.*, vol. 56, no. 4, pp. 3431–3442, Jul./Aug. 2020.
- P. D. Achlerkar, S. R. Samantaray, and M. S. Manikandan, "Variational mode decomposition and decision tree based detection and classification of power quality disturbances in grid-connected distributed generation system," *IEEE Trans. Smart Grid*, vol. 9, no. 4, pp. 3122–3132, Jul. 2018.
- Y. Liu, T. Jin, and M. A. Mohamed, "A novel dual-attention optimization model for points classification of power quality disturbances," *Appl. Energy*, vol. 339, 2023, Art. no. 121011.
- Q. Tang, W. Qiu, and Y. Zhou, "Classification of complex power quality disturbances using optimized S-transform and kernel SVM," *IEEE Trans. Ind. Electron.*, vol. 67, no. 11, pp. 9715–9723, Nov. 2020.
- M. Sahani and P. K. Dash, "Automatic power quality events recognition based on Hilbert Huang transform and weighted bidirectional extreme learning machine," *IEEE Trans. Ind. Informat.*, vol. 14, no. 9, pp. 3849–3858, Sep. 2018.
- K. Thirumala, M. S. Prasad, T. Jain, and A. C. Umarikar, "Tunable-Q wavelet transform and dual multiclass SVM for online automatic detection of power quality disturbances," *IEEE Trans. Smart Grid*, vol. 9, no. 4, pp. 3018–3028, Jul. 2018.
- U. Singh and S. N. Singh, "Optimal feature selection via NSGA-II for power quality disturbances classification," *IEEE Trans. Ind. Informat.*, vol. 14, no. 7, pp. 2994–3002, Jul. 2018.
- K. Zhu, Z. Teng, W. Qiu, Q. Tang, and W. Yao, "Complex disturbances identification: A novel PQDs decomposition and modeling method," *IEEE Trans. Ind. Electron.*, vol. 70, no. 6, pp. 6356–6365, Jun. 2023.
- S. Wang and H. Chen, "A novel deep learning method for the classification of power quality disturbances using deep convolutional neural network," *Appl. Energy*, vol. 235, pp. 1126–1140, 2019.
- R. V. Monteiro, R. F. Teixeira, and A. S. Bretas, "Power quality disturbances diagnosis: A 2D densely connected convolutional network framework," *Electric Power Syst. Res.*, vol. 212, 2022, Art. no. 108252.
- W. Qiu, Q. Tang, J. Liu, and W. Yao, "An automatic identification framework for complex power quality disturbances based on multifusion convolutional neural network," *IEEE Trans. Ind. Informat.*, vol. 16, no. 5, pp. 3233–3241, May 2020.
- A. Vaswani et al., "Attention is all you need," in *Proc. Int. Conf. Neural Inf. Process. Syst.*, 2017, pp. 6000–6010.
- S. Woo, J. Park, J.-Y. Lee, and I. S. Kweon, "CBAM: Convolutional block attention module," in *Proc. Eur. Conf. Comput. Vis.*, 2018, pp. 3–19.
- F. Wang et al., "Residual attention network for image classification," in *Proc. IEEE Conf. Comput. Vis. Pattern Recognit.*, 2017, pp. 3156–3164.

- [28] K. He, X. Zhang, S. Ren, and J. Sun, “Delving deep into rectifiers: Surpassing human-level performance on ImageNet classification,” in *Proc. IEEE Int. Conf. Comput. Vis.*, 2015, pp. 1026–1034.
- [29] L. Stanković, “A measure of some time–frequency distributions concentration,” *Signal Process.*, vol. 81, no. 3, pp. 621–631, 2001.
- [30] A. Moukadem, Z. Bouguila, D. O. Abdeslam, and A. Dieterlen, “A new optimized stockwell transform applied on synthetic and real non-stationary signals,” *Digit. Signal Process.*, vol. 46, pp. 226–238, 2015.
- [31] W. Qiu, Q. Tang, Z. Teng, C. Liang, and W. Yao, “Automatic classification of power quality disturbances via weighted convolutional neural network,” in *Proc. IEEE Power Energy Soc. Gen. Meeting*, 2019, pp. 1–5.
- [32] K. He, X. Zhang, and S. Ren, “Identity mappings in deep residual networks,” in *Proc. Eur. Conf. Comput. Vis.*, 2016, pp. 630–645.
- [33] X. Li, W. Wang, X. Hu, and J. Yang, “Selective kernel networks,” in *Proc. IEEE/CVF Conf. Comput. Vis. Pattern Recognit.*, 2019, pp. 510–519.
- [34] S. Ioffe and C. Szegedy, “Batch normalization: Accelerating deep network training by reducing internal covariate shift,” in *Proc. Int. Conf. Mach. Learn.*, 2015, pp. 448–456.
- [35] A. Stergiou and R. Poppe, “AdaPool: Exponential adaptive pooling for information-retaining downsampling,” *IEEE Trans. Image Process.*, vol. 32, pp. 251–266, 2023.
- [36] *IEEE Recommended Practice for Monitoring Electric Power Quality*, IEEE Power and Energy Society Std., IEEE Standard 1159-2009, 2009.
- [37] R. H. Tan and V. K. Ramachandaramurthy, “Numerical model framework of power quality events,” *Eur. J. Sci. Res.*, vol. 43, no. 1, pp. 30–47, 2010.
- [38] Y. Wang, Q. Li, F. Zhou, Y. Zhou, and X. Mu, “A new method with Hilbert transform and slip-SVD-based noise-suppression algorithm for noisy power quality monitoring,” *IEEE Trans. Instrum. Meas.*, vol. 68, no. 4, pp. 987–1001, Apr. 2019.
- [39] S. Z. Motlagh and A. A. Foroud, “Power quality disturbances recognition using adaptive chirp mode pursuit and grasshopper optimized support vector machines,” *Measurement*, vol. 168, 2021, Art. no. 108461.



**Jun Ma** (Student Member, IEEE) received the B.S. degree in measurement and control technology and instrument in 2019 from Hunan University, Changsha, China, where he is currently working toward the Ph.D. degree in control science and engineering.

Since 2022, he has been a Joint Doctoral Student with the University of Bologna, Bologna, Italy. His current research interests include electrical measurement, intelligent optimization, power quality, and the reliability analysis of power metering equipment.



**Qiu Tang** was born in Hunan, China, in 1970. She received the B.S., M.S., and Ph.D. degrees in electrical engineering from Hunan University, Changsha, China, in 1992, 1995, and 2010, respectively, and the M.Sc. degree in electrical engineering from the University of Nottingham, Nottingham, U.K., in 2005.

Since 2021, she has been a Professor with Hunan University. Her current research interests include power system analysis, digital signal processing, power quality, and virtual instruments.



**Minjun He** received the B.S. degree in electrical engineering and automation from Northeast Agricultural University, Harbin, China, in 2019. He is currently working toward the Ph.D. degree in electrical engineering with Hunan University, Changsha, China.

Since 2022, he has been a Joint Doctoral Student with the University of Bologna, Bologna, Italy. His current research interests include deep learning, power quality measurement, and power data analysis.



**Lorenzo Peretto** (Senior Member, IEEE) received Ph.D. degree in electrical engineering from University of Bologna, Bologna, Italy, in 1997. He is currently a Professor of electrical and electronic measurements with the University of Bologna, Bologna, Italy. He has authored or coauthored more than 200 articles, holds 24 patents, and coauthored three books. He is currently a consultant of industries operating in the field of instrumentation and sensors for electrical measurements. His research interests

include the design and calibration of voltage and current instrument transformers for medium- and high-voltage power networks, the design and realization of calibration systems of voltage and current instrument transformers, and the measurements of electrical quantities in power networks.

Dr. Peretto is a Member of the IEEE Instrumentation and Measurement Society. He is the Chairperson of the Annual IEEE Applied Measurements for Power System Conference, a Member of the IEC TC38 “Instrument Transformers,” and the Chairman of the TC38/WG45 “Standard Mathematical Models for Instrument Transformers” and the TC38/WG53 “Uncertainty Evaluation in the Calibration of Instrument Transformers.”



**Zhaosheng Teng** received the B.Sc., M.Sc., and Ph.D. degrees in electrical engineering from Hunan University, Changsha, China, in 1984, 1995, and 1998.

From 1998 to 2000, he was a Postdoctoral Research Fellow with the National University of Defense Technology, Hunan, China. Since 2000, he has been a Professor with Hunan University. His current research interests include power quality monitoring, information fusion, and electrical measurement.